Study of pinholes and nanotubes in AlInGaN films by cathodoluminescence and atomic force microscopy

M. Herrera, A. Cremades, J. Piqueras, M. Stutzmann, and O. Ambacher

Citation: J. Appl. Phys. **95**, 5305 (2004); doi: 10.1063/1.1690454
View online: http://dx.doi.org/10.1063/1.1690454
View Table of Contents: http://jap.aip.org/resource/1/JAPIAU/v95/i10
Published by the American Institute of Physics.

Study of pinholes and nanotubes in AlInGaN films by cathodoluminescence and atomic force microscopy

M. Herrera, A. Cremades,[a] and J. Piqueras
Departamento de Física de Materiales, Facultad de Ciencias Físicas, Universidad Complutense de Madrid, Madrid 28040, Spain

M. Stutzmann
Walter Schottky Institute, Technical University Munich, Am Coulombwall, D-85748 Garching, Germany

O. Ambacher
Center for Micro- and Nanotechnologies, Technical University Munich, Gustav-Kirchhoff-Str. 7, D-98693 Ilmenau, Germany

(Received 24 November 2003; accepted 9 February 2004)

Cathodoluminescence (CL) in the scanning electron microscope and atomic force microscopy (AFM) have been used to study the formation of pinholes in tensile and compressively strained AlInGaN films grown on Al_2O_3 substrates by plasma-induced molecular beam epitaxy. Nanotubes, pits, and V-shaped pinholes are observed in a tensile strained sample. CL images show an enhanced emission around the pits and a lower intensity at the V-shaped pinholes. Rounded pinholes appear in compressively strained samples in island-like regions with higher In concentration. The grain structure near the pinholes is resolved by AFM. © *2004 American Institute of Physics.*
[DOI: 10.1063/1.1690454]

INTRODUCTION

The fabrication of devices based on III–V nitrides has attracted increasing attention in the last few years. In particular, InGaN/GaN and AlGaN/GaN quantum well structures have been used in light emitting diodes (LEDs) as well as in active regions of pulsed and continuous wave laser diodes[1] (LDs). However, there are problems to control the electronic and structural quality of the films of these ternary compounds mainly due to composition fluctuations, dislocations,[2] pinholes,[3] and cracks,[4] which have been observed in films grown on different substrates and buffer layers.

In an attempt to solve these problems, several authors have grown quaternary films of AlInGaN by chemical vapor deposition (CVD)[5–9] and molecular beam epitaxy (MBE).[10] The desired band gap of the quaternary semiconductors can be adjusted, independently from the lattice constant, by controlling the atomic composition in the growth process. This flexibility allows the lattice strain of heterostructures (e.g., InGaN quantum wells with AlInGaN barriers) to be varied between compressive, zero, and tensile strain. Enhanced crystal quality has been observed in quantum heterostructures of AlInGaN/InGaN,[11,12] and the piezoelectric field produced by the strain was eliminated[13] by using lattice matched AlInGaN/InGaN templates.

However, to obtain these quaternary compounds the growth temperature is a very critical parameter due to the large difference in the vapor pressure between Al and In. Low growth temperature leads to low crystalline quality while high temperature increases the vaporization of In.[10] We have reported competitive incorporation effects of In and Al in quaternary samples obtained at different temperatures[14] on a 500 nm thick GaN buffer layer. Our results showed that built-in strain in the layers determines the preferential incorporation of In atoms into the alloy in regions where the strain is relaxed via the formation of pinholes. The luminescence emission is not only influenced by the In content but also by the misfit strain in the films.

In this work a series of AlInGaN samples grown by MBE[10] on a 1.8 μm thick GaN buffer layer were analyzed by Cathodoluminescence (CL), Atomic Force Microscopy (AFM), and X-ray microanalysis in order to study strain-induced effects on the defect structure and luminescence properties of these quaternaries.

EXPERIMENTAL DETAILS

The samples investigated were hexagonal AlInGaN films grown on Al_2O_3 substrates by plasma-induced molecular beam epitaxy. To obtain different alloy compositions, the flux of Ga and the growth temperature were changed. The heterostructures consists of a thin, about 5 nm, AlN nucleation layer grown on a c-Al_2O_3 substrate to ensure metal face (instead of nitrogen face) polarity, followed by a 1.8 μm GaN buffer layer and 200 nm of $Al_xIn_yGa_{1-x-y}N$. A relatively thick GaN layer (the GaN thickness is high enough for the layer to be fully relaxed) is used as a buffer to avoid as much as possible defect generation related to interface roughness and in order to improve the microstructure of the quaternary film. Further growth details are given in Ref. 10. Previous Rutherford backscattering spectroscopy (RBS) results of the samples are summarized in Table I. The large mismatch of lattice constants and thermal expansion coefficients of the different nitride layers can result in significant biaxial stress in the heterostructures, causing strong piezo-

[a]Electronic mail: cremades@fis.ucm.es

TABLE I. Growth temperature, experimental compositions of the alloys obtained by RBS, and residual stress values σ_{xx}.

Sample	Growth temperature (°C)	Al (%)	In (%)	Ga (%)	$\sigma_{xx}=\frac{a_{\text{sustrate}}}{a_{\text{film}}}-1$
1	745	11.0	1.5	87.0	9.4×10^{-4}
2	745	13.4	2.3	84.7	6.3×10^{-4}
3	685	12.4	6.9	80.7	-5×10^{-3}

electric fields and a decrease of light intensity emitted by the active regions of GaN-based LEDs and LDs. Assuming that a solid solution of InN, AlN, and GaN is present in these quaternaries,[10] the ratio of the concentration of In:Al for lattice matching with GaN can be estimated from the Vegard Law. By using the values of lattice constants $a_{\text{InN}}=3.548$ Å, $a_{\text{AlN}}=3.112$ Å, and $a_{\text{GaN}}=3.189$ Å, this ratio In:Al is found to be around 1:4.7. Sample 2 of Table I is near to be lattice matched with the relaxed GaN buffer layer (In:Al=1:5.8), whereas sample 1, with the lower In content, presents tensile strain and sample 3, with the highest In content, experiences compressive strain. The stress values calculated from the relationship $\sigma_{xx}=a_{\text{substrate}}/a_{\text{film}}-1$ are also shown in Table I.

The CL study was carried out using a Leica S440 SEM at 77 K, with low electron beam energies between 3 and 5 keV in order to obtain luminescence only from the quaternary film (the estimated penetration range is about 160 nm for 5 keV). For light detection a Hamamatsu R928 photomultiplier was applied. A Park Scientific Instruments Autoprobe CP was used in the AFM measurements, and the x-ray-microanalysis were carried out by EDS in a JEOL JXA-8900M super probe.

RESULTS

AFM measurements show that the quaternary films exhibit by a grain structure with grain sizes in the range of 0.5–1 μm (Fig. 1). The AFM images of sample 1 show a distribution of two different kinds of pits at the surface, labeled, respectively, A and B in Fig. 1(a). The A pits appear as rounded features (labeled A) with a size of about 600 nm emerging in regions between grains, while the pits labeled B are observed as 100–300 nm wide holes with sharp corners and curved sides occurring at grain sides. The AFM line profiles for A pits do not show any bumps on the sides and the walls fall off with a small slope, as shown in Fig. 1(b). On the contrary, the AFM line profiles for B pits are composed by two bumps revealing the accumulation of material at the pit border, and abrupt pit walls, as observed in Fig. 1(c). The pit width has been obtained by measuring the distance between the peaks of the bumps in the AFM profiles. For sample 1, corresponding to the lowest In concentration and in-plane tensile strain, both kind of pits are randomly distributed. Some surface areas are relatively smooth, while others tend to have a high density of pits. The averaged densities of A and B pits, calculated from AFM images of sample 1, are of the order of 1×10^7 and 2.5×10^7 cm^{-2}, respectively. B pits are absent in the samples 2 and 3, while islands protruding about 130 nm from the surface background appear around some A pits, as shown in Figs. 2(a) and 2(b). The density of islands varies from 1.7×10^7 cm^{-2} for sample 2 with an intermediate indium concentration, to 7.6×10^5 cm^{-2} for sample 3. This result can be explained in terms of the island size that increases from 2.5–5 μm for sample 2 to 10–20 μm for sample 3. The rms roughness of the films surface increases with the final indium composition. Typical values calculated from AFM images are around 13 nm for sample 1, 36 nm for sample 2, and 41 nm for sample 3.

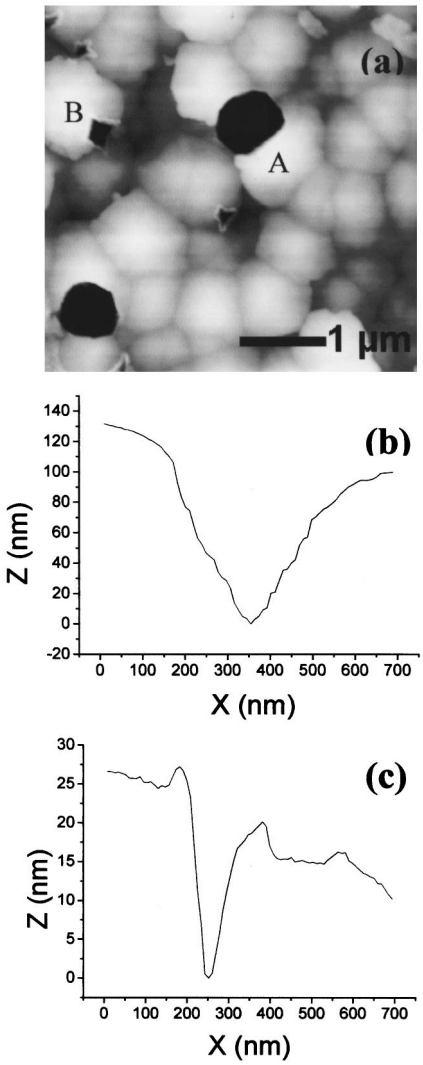

FIG. 1. (a) AFM image of sample 1, showing the grain structure of the film. A V-shaped pinhole and a pit are labeled as A and B, respectively. AFM profiles through (b) a pinhole and (c) a pit, for an illustration.

In the secondary electron image of sample 1 shown in Fig. 3(a), it is observed that A pits (hereinafter referred to as pinholes[3]) emerge with a V shape with a small hole of about 75 nm in the center while the B pits (hereinafter for simplicity referred to as pits) appear as holes with diameters smaller than 300 nm and sharp corners without any marked surface feature around the emergence point. Cross-sectional SEM observations of sample 1 reveal the occurrence of nanotubes extending along the quaternary and the GaN buffer films, which sometimes emerge opening out about 300 nm at the

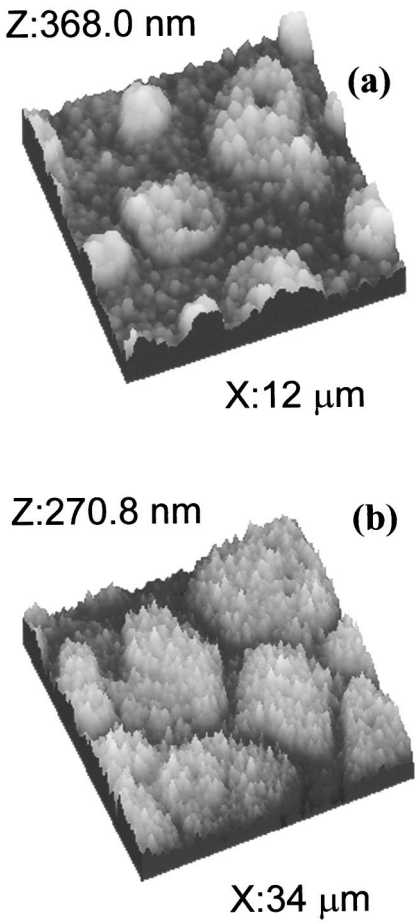

FIG. 2. (a) and (b) AFM images of In-rich samples 2 and 3, containing only V-shaped pinholes and showing island formation and increasing roughness.

surface [arrows in Fig. 3(b)]. Figure 3(c) shows the CL image of the area shown in Fig. 3(a). An enhanced CL emission is observed around the pits, some of them marked with arrows, while a lower intensity is associated to the region

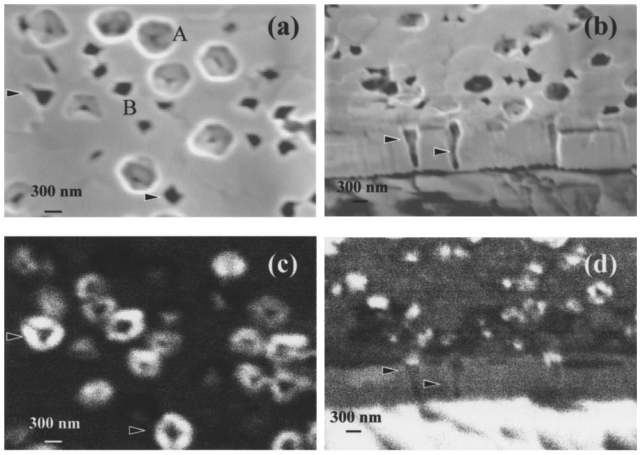

FIG. 3. (a) Secondary electron image (SE) of the surface of sample 1, showing pinholes (A) and pits (B). (b) SE of the cross-section of the quaternary film. Some nanotubes emerge at the surface as V-shaped pinholes (marked by arrows in the image). (c) CL image of the region (a) showing higher intensity around pits (some of them marked with arrows). (d) CL image of region (b). Around nanotubes no emission is observed.

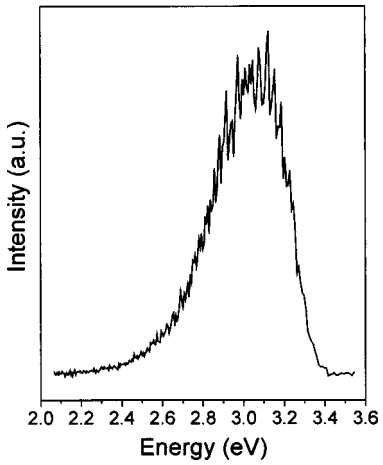

FIG. 4. CL spectrum of sample 1.

around the small holes located at the apex of pinholes. The CL image [Fig. 3(d)] of the cross-section presented in Fig. 3(b) shows that there is no CL emission associated with the nanotubes in the GaN buffer layer but enhanced CL intensity is observed at the quaternary film surface. Therefore the 300 nm wide pits seem to be formed by the emergence of the nanotubes at the quaternary surface. CL spectra recorded in different points of the surface show similar spectra in the pinholes and pits and in the sample background, although with different intensities (Fig. 4). The spectra consist of a broad emission centered at 3.1 eV. X-ray mapping shows a reduced concentration of In around the pinholes and pits (Fig. 5).

In sample 2 and in the compressively strained sample 3, the pinholes appear on islands as the SE images of Figs. 6(a) and 6(b), corresponding, respectively to samples 2 and 3, show. The higher CL emission of the islands, observed in Figs. 6(c) and 6(d), could be caused by diffusion of carriers toward these features prior to recombination. The local CL spectra of the islands show a red shift of the peak energy of about 200 and 100 meV for the samples 2 and 3, respectively (Fig. 7).

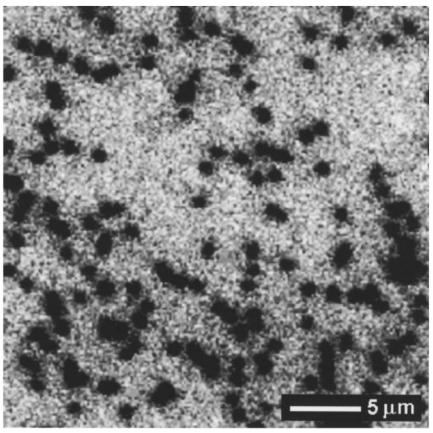

FIG. 5. X-ray mapping of ln sample 1. The dark regions correspond to pinholes.

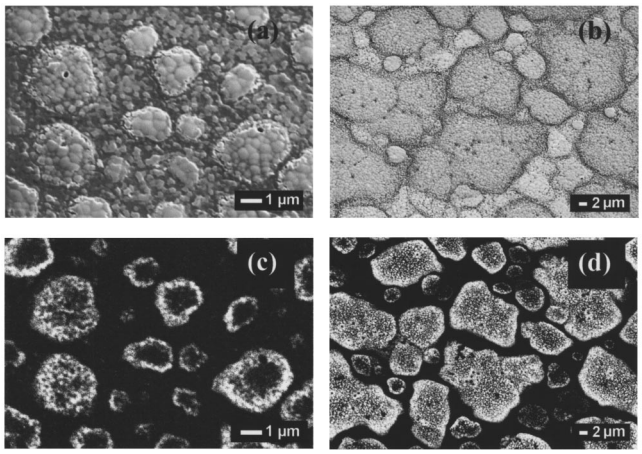

FIG. 6. (a) and (b) SE images of samples 2 and 3, respectively. Pinhole formation is observed on the islands of these two samples. (c) and (d) show the corresponding CL images. Islands show higher CL emission than the background.

DISCUSSION

Due to the large lattice mismatch and thermal expansion coefficient difference between the epilayer and the substrate, nitride films exhibit a high density of defects, namely threading dislocations, pits, nanotubes, and stacking faults. For InGaN and GaN films V-shaped pinholes are commonly observed.[2,15] Pinholes are open hexagonal inverted pyramids defined by the six {10−11} planes, and are reported to originate from either threading dislocations,[15] stacking mismatch boundaries induced by stacking faults due to strain relaxation[16] or from slow growth rate on polar (10−11) planes induced by impurity poisoning of growth steps or any development of surface roughness during growth.[17]

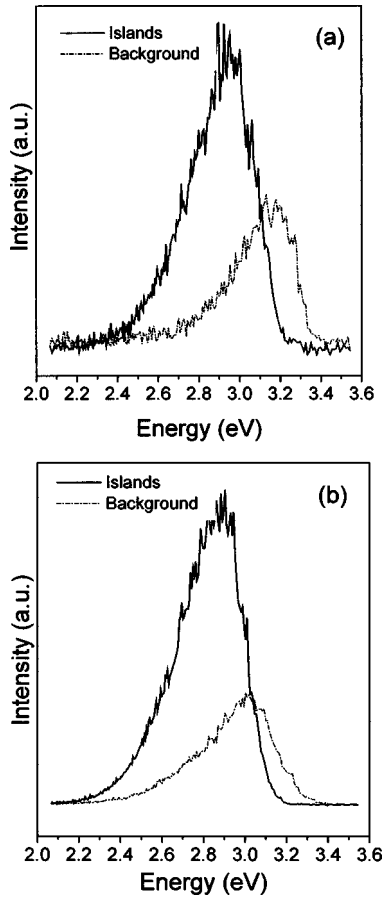

FIG. 7. CL spectra of (a) sample 2 and (b) sample 3. A shift of the energy peak is observed between the emissions of island and background in both cases.

Liliental-Weber *et al.*[17] have studied the formation of V-shape pinholes, related to V-shape facets in (10−11) polar planes and nanotubes with (10−10) facets, in tensile strained GaN films. Their results indicate that the origin of these defects may be related to growth kinetics on particular crystallographic planes, and impurity poisoning of growth steps. In fact, x-ray mapping has been found to show a reduced concentration of In and Ga in pinholes and nanotubes (Fig. 5). The higher CL emission around the pits, as compared with that of the V-shape pinholes could be related to different impurities or point defect agglomeration around both kinds of features. The occurrence of nanotubes in hexagonal films seems to follow a strain relaxation process. In AlGaN films grown over GaN, a direct relation between the formation of deep pinholes and Al concentration, or tensile strain, has been reported.[18] Inhomogeneous strain around the nanotubes can lead to the accumulation of point defects in similar way to what is observed around an indentation.[19] In a previous work on GaN/InGaN structures,[20] a similar distribution of small and large pits were observed on the surface of a 30 nm GaN capping layer. TEM studies showed that the pits were mostly associated with threading defects, including nanotubes. The nanotubes were hollow tubes with diameters 5–30 nm and {10−10} facetted sides, and some of them were hollow core screw dislocations with Burgers vectors $b=\pm c$. No correlation was found between the overall density of dislocations and the density of nanotubes and pinholes. The nanotubes observed in our samples may grow from pinholes present during early stages of growth, and often open out into larger pits at the surface lowering the total energy by relieving the strain energy at the expense of free surface energy, as observed in the cross section of the tensile strained film. It seems that dislocations sometimes associated with these hollow defects are not related to the nucleation of pinholes or nanotubes, but rather they are attracted to them to reduce line energy.[20] The nanotubes observed in the cross section of our samples extend along the *c* axis through the whole thickness of the quaternary and buffer films. This may be an indication that these nanotubes line up with others along straight threading dislocations formed at the GaN/Al_2O_3 interface, or may develop from a pinhole that occurred in the first GaN layers.

According to our previous results, the islands formation is due to the competitive incorporation of In and Al in the film.[14] X-ray measurements in both samples show a higher In concentration in the islands. Indium atoms tend to segregate during growth to the six {10−11} planes to reduce the deformation energy due to the lattice mismatch. By increasing the indium content in the alloy, the lattice mismatch increases and, therefore, more deformation energy needs to be relieved. This fact may induce the formation and further growth of the indium-rich island around pinholes. Elastic

relaxation through three-dimensional 3-D is landing has been observed in a variety of systems, such as Si–Ge or InAs/GaAs.[21] This process of elastic relaxation is typical of a Stransky–Krastanov growth mode. During an early stage, the growth remains two dimensional until a critical thickness is reached and a transition to a three-dimensional mode occurs. At this stage the roughness increases and the lattice parameter rises toward a value closer to that of the relaxed material. The free surface of the islands contributes to elastic relaxation of the strain. Therefore the observed increase in the surface roughness of the quaternary films is related to the island growth. The roughness does not increase linearly with the In content as the coalescence of the islands increases. As in the tensile strained films, the occurrence of pinholes in compressively strained films has been explained by strain relaxation mechanisms.[22,23] The pinhole formation in the islands would be related to their higher compressive strain.

Free carrier recombination exhibits a similar behavior at small pits and at larger pinholes of sample 1. Small pits are surrounded by a bright CL halo, showing a dark core, whereas at pinholes a less intense luminescence is observed, indicating a lower recombination rate of free carriers. Free carrier recombination may be enhanced at these defect sites degrading both the electrical and optical properties of these materials. Deep level emission at around 3.1 eV was previously observed for similar AlInGaN films,[9,14] and was related to nonoptimum growth conditions for Al-containing alloys.

A reduction of the band gap is expected in the islands due to their nonoptimum-enhanced In concentration.[24,25] The red shift of the peak energy observed in the local CL spectra of Fig. 7 is an indication of the effective incorporation of In to the alloy in samples with a higher In content. In contrast to samples grown on a thin GaN buffer layer, these samples do not show a common emission at about 3.1 eV, as for sample 1, but an emission that varies consistently with the In concentration. No bandgap edge emission is observed in the range estimated by the Vegard's law, even including the bowing parameter (b) corrections from Ref. 9 (b_{AlGaN} equal to -1 eV, b_{InGaN} ranged from -1 to -4.8 eV, and b_{AlInN} equal to -5 eV). Taking into account that the bowing parameters given for InGaN and AlInN are based on a value of the InN bandgap of about 1.9 eV and recent experiments prove the InN bandgap to be about 0.7 eV,[26] the bowing parameters of the ternaries given in Ref. 9 should be revised. The deviation suggests the possibility of composition-dependent bowing parameters. Indeed, evidence for such behavior has already been provided for InGaN.[25]

CONCLUSIONS

In summary, the appearance of pinholes and pits in AlInGaN films has been investigated by a combination of CL, AFM, and x-ray microanalysis. Different pinholes are identified in the tensile and compressively strained samples. V-shaped pinholes, pits and, nanotubes appear in tensile strained films, and their formation seems to be related with the presence of impurities or point defects. CL images show a higher emission around the pits than in the V-shaped pinholes, revealing a different defect distribution in the surroundings of both kinds of features.

In and Al show competitive incorporation in the quaternary films, inducing In-rich regions. Circular pinholes appear in In-rich islands of compressively strained and low tensile strained films. An effective incorporation of In to the alloys is obtained, as revealed by the shift of the CL emission peaks in In-rich samples. The incorporation of In in the alloy results in an increase of the emission intensity. In order to achieve a InAlGaN quaternary alloy emitting close to the GaN band edge emission (3.45 eV) needs at least 3%–5% of In incorporation as well as higher Al content, because InAlGaN shows a large band bowing. The use of a thicker substrate does not suppress the compositional inhomogeneities, and results in an incorporation of a smaller In fraction in the alloy.

ACKNOWLEDGMENTS

This work has been partially support by the MCYT (Project No. MAT-2000-2119). M. H. thanks CONACYT for a postdoctoral grant. The help of Dr. Hidalgo in the experimental measurements is acknowledged.

[1] S. Nakamura, S. Pearton, and G. Fasol, *The Blue Laser Diode* (Springer-Verlag, Berlin, 2000).
[2] A. Cremades and J. Piqueras, Mater. Sci. Eng., B **91**, 341 (2002).
[3] A. Cremades, J. Piqueras, M. Albrecht, M. Stutzmann, and H. P. Struck, Mater. Sci. Eng., B **80**, 313 (2001).
[4] S. Einfeld, M. Dieβelberg, H. Heinke, D. Hommel, D. Rudloff, J. Christen, and D. F. Davis, J. Appl. Phys. **92**, 118 (2002).
[5] F. G. McIntosh, K. S. Boutros, J. C. Roberts, S. M. Bedair, E. L. Piner, and N. A. El-Masry, Appl. Phys. Lett. **68**, 40 (1996).
[6] M. Asif Khan, J. W. Yang, G. Simin, R. Gaska, M. S. Shur, Hans-Conrad zur Loye, G. Tamulaitis, A. Zukauskas, D. J. Smith, and D. Chandrasekhar, Appl. Phys. Lett. **76**, 1161 (2000).
[7] J. Zhang, J. Yang, G. Simin, M. Shatalov, M. A. Khan, M. S. Shur, and R. Gaska, Appl. Phys. Lett. **77**, 2668 (2000).
[8] G. Tamulaitis, K. Kazlauskas, S. Jursenas, A. Zukauskas, M. A. Khan, J. W. Yang, J. Zhang, G. Simin, M. S. Shur, and R. Gaska, Appl. Phys. Lett. **77**, 2136 (2000).
[9] M. E. Aumer, S. F. LeBoeuf, F. G. McIntosh, and S. M. Bedair, Appl. Phys. Lett. **75**, 3315 (1999).
[10] A. P. Lima, C. R. Miskys, U. Karrer, O. Ambacher, A. Wenzel, B. Rauschenbach, and M. Stutzmann, J. Cryst. Growth **220**, 341 (2000).
[11] A. Chitnis, A. Kumar, M. Shatalov, V. Adivarahan, A. Lunev, J. W. Yang, G. Simin, and Asif Khan, Appl. Phys. Lett. **77**, 3800 (2000).
[12] J. Zhang, J. Yang, G. Simin, M. Asif Khan, M. S. Shur, and R. Gaska, Appl. Phys. Lett. **77**, 2668 (2000).
[13] M. E. Aumer, S. F. LeBoeuf, B. F. Moody, and S. M. Bedair, Appl. Phys. Lett. **79**, 3803 (2001).
[14] A. Cremades, V. Navarro, J. Piqueras, A. P. Lima, O. Ambacher, and M. Stutzmann, J. Appl. Phys. **90**, 4868 (2001).
[15] Y. Chen, T. Takeuchi, H. Amano, I. Akasaki, N. Yamada, Y. Kaneko, and S. Y. Wang, Appl. Phys. Lett. **72**, 710 (1998).
[16] H. K. Cho, J. Y. Lee, G. M. Yang, and C. S. Kim, Appl. Phys. Lett. **79**, 215 (2001).
[17] Z. Liliental-Weber, Y. Chen, S. Ruvimov, and J. Washburn, Phys. Rev. Lett. **79**, 2835 (1997).
[18] L. Geng, F. A. Ponce, S. Tanaka, H. Omiya, and Y. Nakagawa, Phys. Status Solidi A **188**, 803 (2001).
[19] M. Herrera Zaldívar, P. Fernández, and J. Piqueras, Semicond. Sci. Technol. **13**, 900 (1998).
[20] D. Cherns, J. Phys.: Condens. Matter **12**, 10 205 (2000).
[21] J. M. Moison, F. Houzay, F. Barthe, L. Leprince, E. Andre, and O. Vatel,

Appl. Phys. Lett. **64**, 196 (1994).
[22] L. Shi, C. D. Poweleit, F. A. Ponce, J. Menendez, and W. W. Chow, Appl. Phys. Lett. **79**, 75 (2001).
[23] B. Jahnen, M. Albrecht, W. Dorsch, S. Christiansen, H. P. Strunk, D. Hanser, and R. F. Davis, MRS Internet J. Nitride Semicond. Res. **3**, 39 (1998).
[24] C. A. Parker, J. C. Roberts, S. M. Bedair, M. J. Reed, S. X. Liu, and N. A. El-Masry, Appl. Phys. Lett. **75**, 2776 (1999).
[25] M. D. McCluskey, A. G. Van de Walle, C. P. Master, L. T. Romano, and N. M. Johnson, Appl. Phys. Lett. **72**, 2725 (1998).
[26] J. Wu, W. Walukiewicz, W. Shan, K. M. Yu, J. W. Ager, III, S. X. Li, E. E. Haller, H. Lu, and W. J. Schaff, J. Appl. Phys. **94**, 4457 (2003).